Anai *et al. Earth, Planets and Space (2023) 75:24*
https://doi.org/10.1186/s40623-023-01783-x

Earth, Planets and Space

EXPRESS LETTER

Open Access

Temporal change in rock-magnetic properties of volcanic ashes ejected during a 1-year eruption event: a case study on the Aso Nakadake 2019–2020 eruption

Chisato Anai[1,2*], Takahiro Ohkura[1], Shin Yoshikawa[1] and Nobutatsu Mochizuki[3]

Abstract

We investigated temporal changes in the rock-magnetic properties of volcanic ash ejected from the Aso Nakadake volcano during a sequence of ash eruptions from 2019 to 2020. For 39 volcanic ash samples, magnetic hysteresis parameters, including saturation magnetization (M_s), saturation remanent magnetization (M_{rs}), coercivity (B_c), and coercivity of remanence (B_{cr}), were obtained. Curie temperature (T_c) of the samples was also estimated using thermomagnetic analyses. Titanium-rich and -poor titanomagnetites were the dominant magnetic minerals in the volcanic ash, of which the titanium-rich phase was dominant. Systematic magnetic measurements of the volcanic ash ejected during the 1-year eruption event indicate that temporal changes in the hysteresis parameters occurred throughout the event. These temporal changes suggest that the M_{rs}/M_s and B_c values of the volcanic ash increased considerably during several periods. The clear increases in M_{rs}/M_s and B_{cr}, associated with the central peak in FORC diagrams, indicate that non-interacting single-domain grains increased. For these high M_{rs}/M_s and B_c samples, thermal demagnetizations of 3-axis IRM show that the low unblocking-temperature component up to 250–300 °C has apparently higher coercivity, suggesting that the above-mentioned, non-interacting single-domain grains are Ti-rich titanomagnetite. Interestingly, the high M_{rs}/M_s and B_c values were synchronous with observations of volcanic glow. These results suggest that changes in the magnetic properties of titanomagnetite grains in volcanic ash reflect changes in physical conditions from the vent to the conduit of the volcano.

Keywords Coercivity, Saturation magnetization, Saturation remanent magnetization, Single domain, Volcanic ash, Aso Nakadake volcano

*Correspondence:
Chisato Anai
chisato@kochi-u.ac.jp
Full list of author information is available at the end of the article

Graphical Abstract

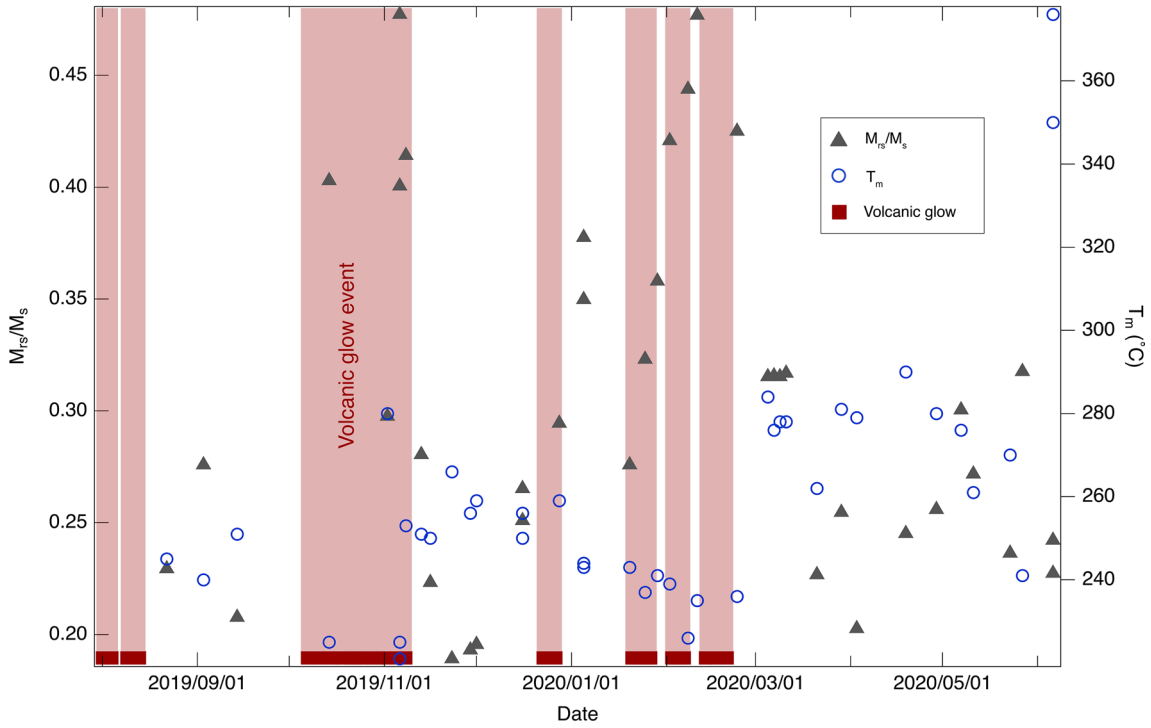

Introduction

Paleomagnetism recently have been applied to make new contributions to volcanology. In particular, estimates of eruption ages and/or classification of volcanic ejecta using paleosecular variations in paleomagnetic direction have contributed greatly to the improvement of high-resolution volcanic stratigraphy (e.g., Anai et al. 2021). Meanwhile, only a few studies have linked eruptive activity to rock magnetism (e.g., Knnot et al. 2020; Risica et al. 2020).

The magnetic minerals in volcanic ash are usually dominated by titanomagnetite (e.g., Dunlop and Özdemir 1997). Notably, the composition of titanomagnetite reflects the oxygen fugacity and temperature during crystallization (Buddington and Lindsley 1964). Therefore, the magnetic properties of titanomagnetite can reflect the conditions present during its eruption. However, previous studies estimating the physical conditions inside a conduit have used relatively slow cooling times, while ejecta from continuous eruptions do not necessarily reflect a single physical condition. Bowles et al. (2013) and Jackson and Bowles (2014) demonstrated post-depositional compositional changes in magnetic minerals in pyroclastic flow deposits through extensive rock-magnetic experiments. These studies found that, even at lower temperature conditions (~400 °C), cation ordering increased and the titanium (Ti) content changed. This compositional change may record information about the magma surface phenomena inside the shallow region of the volcanic conduit.

Magnetic properties vary with composition, grain size, and shape (Dunlop and Özdemir 1997). Grain size is a particularly important factor, single-domain grains governed by shape anisotropy have a ratio of saturation remanent magnetization to remanent magnetization (M_{rs}/M_s) close to 0.5 and a ratio of coercivity of remanence to coercivity (B_{cr}/B_c) close to 1. The grain-size distribution of dominant magnetic mineral can be estimated by obtaining the parameters of their hysteresis measurements combined with first order reversal curve (FORC) diagram. Hysteresis data for volcanic ash would provide the temporal variations in properties (composition, grain size, and shape) of the magnetic minerals.

In this study, we revealed temporal changes in the rock magnetic properties (grain size and/or composition) and discuss the relationship to volcanic phenomena based on detailed magnetic measurements of volcanic ash ejected by intermittent magmatic eruptions that occurred from July 2019 to June 2020 at Aso Nakadake volcano.

The 2019–2020 eruption of Aso Nakadake volcano

Aso Nakadake volcano, which is the only active central cone inside the Aso caldera, is one of the most active volcanoes in Japan (see the Additional file 1 for a detailed description). Magmatic activity at the first crater of the Nakadake volcano in Aso began on July 26, 2019 and continued until June 2020, with several pauses. Increases in volcanic gases and volcanic glow were observed during the active period, in addition to a large amount of ashfall (Japan Meteorological Agency (JMA) 2021; Miyabuchi et al. 2021). Volcanic glow occurs when clouds and plumes above a crater are brightly illuminated by hot magma or volcanic gas in the crater or at the top of the crater (JMA 2021). Volcanic glow is generally observed at night with a highly sensitive camera, and was observed continuously at Aso Nakadake in mid-October 2019 and from early to mid-February 2020. However, the physical mechanism that causes volcanic glow remains unclear.

A series of continuous ash eruptions occurred in 2019–2020 as part of the typical eruptive cycle (see Additional file 1: Fig. S1) of Aso Nakadake volcano. Volcanic gas plumes, seismicity, infrasound, and the total geomagnetic field are monitored at Aso Nakadake volcano by Kyoto University and the Japan Meteorological Agency (JMA). A detailed study of the eruption of Aso Nakadake volcano was also conducted to analyze the discharged mass and the components of the tephra-fall deposits (Miyabuchi and Hara 2019). Systematic analyses of temporal changes in the rock-magnetic properties of the volcanic ash throughout the eruption have not been performed for eruptions prior to 2019. However, since the grain sizes and composition of magnetic minerals in volcanic ash are thought to reflect the ambient temperature gradients and pressure conditions during eruption, rock magnetic analyses have the potential to infer temporal changes in physical conditions inside the crater.

Sample

Volcanic ash samples were collected from eight sites including the observation points established by the Aso Volcanological Laboratory, Kyoto University. In this study, we focused on volcanic ash collected at four sampling sites: Kako-fuchi (KAF), Hondo observatory (HOND), Sakanashi (SAK), and National Aso Youth Friendship Center (AYFC), which are located approximately 250 m WSW, 1000 m SW, 7000 m NE, and 4400 m NNE of the first crater of the Nakadake volcano, respectively (Additional file 1: Fig. S2). We collected volcanic ash at the KAF and HOND sites that had fallen on solar panels used for the volcano monitoring equipment. At the SAK and AYFC sites, ash samples were collected from the ash that accumulated on the windshield of a car. Ash samples were collected approximately 24 h after the ashfalls were observed, which is quasi-real time to the individual eruptions. Notably, the ashfalls occurred after individual ash eruptions during the 1-year eruption period.

Methods

The collected ash samples were washed with deionized water using an ultrasonic cleaner for 10 min and dried at 60 °C for 2 h. Various rock-magnetic analyses were made on the ash samples. Thirty-nine samples were used for the measurements: 22 samples from KAF, 11 samples from SAK, 5 samples from HOND, and 1 sample from AYFC.

Thermomagnetic analysis yields a diagram of strong-field magnetization vs. temperature, which provides Curie temperature (T_c) phases that can be linked to magnetic minerals and their amounts of each phase. For the thermomagnetic analyses, we used a thermomagnetic balance (NMB-2000 M: Natsuhara Giken, Japan) at Kumamoto University. The measurement conditions were as follows: a maximum temperature of 600 °C, a hold time of 60 s, a heating/cooling rate of 10 °C/min, and an applied field of 0.3 T. Heating/cooling cycles were performed in the air and vacuum atmospheres. For 10 samples, measurements were performed in both air and vacuum atmospheres, but they did not show any notable difference (Additional file 1: Fig. S3). Therefore, the other samples were measured in air. The T_c was determined using the intersecting tangents method which is intersection point of the two tangents to the thermomagnetic curve that bounds the Curie temperature (Grommé et al. 1969).

Thermal demagnetization curves of laboratory-acquired remanence are useful, as they show unblocking-temperature distribution that is linked to T_c. Thermal demagnetization of 3-axis composite isothermal remanent magnetization (IRM) (Lowrie 1990) was performed on ash samples packed in cylindrical quartz cups (depth: ~ 20 mm, inner diameter: ~ 22 mm). Because the volcanic ash was not consolidated, the sample was placed halfway into the quartz cylindrical cup, and the upper space was filled with glass wool to hold the sample in place. IRM measurements of the samples were performed using a pulse magnetizer (MMPM10, Magnetic Meas. Ltd., UK) at the Center for Advanced Marine Core Research, Kochi University (KCC). A pulse magnetic field of 1 T was applied along the axis of the cup (z-axis), a field of 0.3 T was subsequently applied to the y-axis, and a field of 0.1 T was applied to the x-axis. Progressive thermal demagnetization was performed to check the changes in the three components of IRM acquired after the treatment. This method can estimate magnetic minerals as remanence carriers based on the unblocking

curves for three different coercivity components ($\leq$0.1 T, 0.1–0.3 T, and 0.3–1 T).

Hysteresis measurements and back field demagnetization were performed using a vibrating sample magnetometer (VSM; model 3900, Lake Shore (PMC), USA) at KCC. For all of the ash samples, hysteresis loops were measured with a maximum field of 1 T. Hysteresis loops are characterized by three parameters that contribute to estimating the domain state of magnetic minerals: saturation magnetization (M_s), saturation remanent magnetization (M_{rs}), and coercivity (B_c). When a magnetic field is applied to a sample and the field strength increases, the magnetization of the sample also increases. M_s is the state in which, when the magnetic field is increased further, the rate of increase in magnetization slows down and finally reaches practically saturation. This corresponds to a state, where the magnetization of all the magnetic minerals in the sample are parallel to the magnetic field. M_s is determined for each magnetic mineral, e.g., it is 480 kA/m for magnetite and 2.5 kA/m for hematite (Dunlop and Özdemir 1997). Therefore, the volume concentration of magnetic minerals in a sample can be calculated from the value of M_s if the mineral species have been determined independently. After reaching saturation magnetization, the magnetic field is damped back to zero, but the magnetization remains (i.e., M_{rs}). M_{rs} is strongly dependent on magnetic mineral type and on the magnetic domain structure, which is closely related to grain size. As the magnetic field increases in the opposite direction, magnetization gradually decays to zero. The strength of the magnetic field at this point is defined as B_c. Increases in B_c indicate that enhanced stability of the magnetic minerals. M_s, M_{rs}, and B_c were obtained for all samples after correcting the paramagnetic linear contribution.

Back field demagnetization curves were measured after applying a strong field (1 T) which gives M_{rs} to the sample. The sample was progressively demagnetized by applying a direct current back field. The field at which the remanence was demagnetized to zero is call as coercivity of remanence (B_{cr}).

First-order reversal curve (FORC) measurements were also performed for all samples using VSM at KCC. FORC analyses provide information about the magnetic responses of all grains in a sample in terms of their magnetization, represented by the magnitude of the FORC distribution, and the coercivity and magnetic interaction field distributions (shown by the B_c and B_u axes of the FORC diagram, respectively), in which contrasting features can be used to diagnose the full range of magnetic domain states in fine magnetic grain systems (Roberts et al. 2018).

Microscopic observations and semi-quantitative analyses were conducted on two samples (2019.09.14_KAF and 2019.10.14_KAF) by field emission scanning electron microscope (FE–SEM: JSM-7001F, JEOL Ltd., Japan) with an energy dispersive spectroscopy (EDS) system (Aztec-Energy, Oxford Instruments, UK) at Kumamoto University. The accelerating voltage, beam current, and beam size is 15 kV, 1 nA, and < 1 μm, respectively.

Results

Thermomagnetic analyses are performed for all of the volcanic ash samples and two examples are shown in Figs. 1a, b, Additional file 1: Figs. S3 and S4. For a few exceptions, most of the thermomagnetic curves are characterized by two T_c phases (Additional file 1: Figs. S3, S4). The low T_c is 200–350 °C, which is regarded as Ti-rich titanomagnetite with ulvöspinel content x = 0.4–0.6 (Hunt et al. 1995). The high T_c is about 500 °C, which is considered as Ti-poor titanomagnetite with x ~ 0.1. Ti contents of titanomagnetite estimated are included in Additional file 1: Table S1. It should be notified that approximately 60–80% of the strong-field magnetization at room temperature is lost below the low T_c (Fig. 1a, b). Therefore, the dominant magnetic phase for the ash samples of this study is low T_c phase of 200–350 °C.

We observed two exceptional thermomagnetic results that show only a high T_c phase of ~ 500 °C. These two samples did not contain a low T_c phase of 200–350 °C, which was observed for the other samples. The two samples were collected just before the eruption ceased in June 2020.

Thermal demagnetizations of the 3-axis IRM also show two unblocking-temperature ranges of 200–300 °C and 500–600 °C (Fig. 1c, d and Additional file 1: Fig. S5), where the low unblocking-temperature component is dominant. These two unblocking-temperature components should be carried by the two T_c phases, which are recognized in the thermomagnetic curves (Fig. 1a, b). Throughout the eruption period, the low unblocking-temperature component, carried by the low T_c phase, is dominant. It should be noted that the coercivity of the low unblocking-temperature component varies with the eruption period. For the sample of September 14, 2019, the low coercivity component of $\leq$0.1 T (Fig. 1c) is dominated in the low unblocking-temperature component of 200–300 °C, whereas for the sample of October 14, 2019, the low unblocking-temperature component demonstrates a higher coercivity distribution: the middle coercivity component of 0.1–0.3 T is dominant, the low coercivity component of $\leq$0.1 T is smaller than the middle coercivity component, and the high coercivity component of 0.3–1 T is small but can be identified (Fig. 1d).

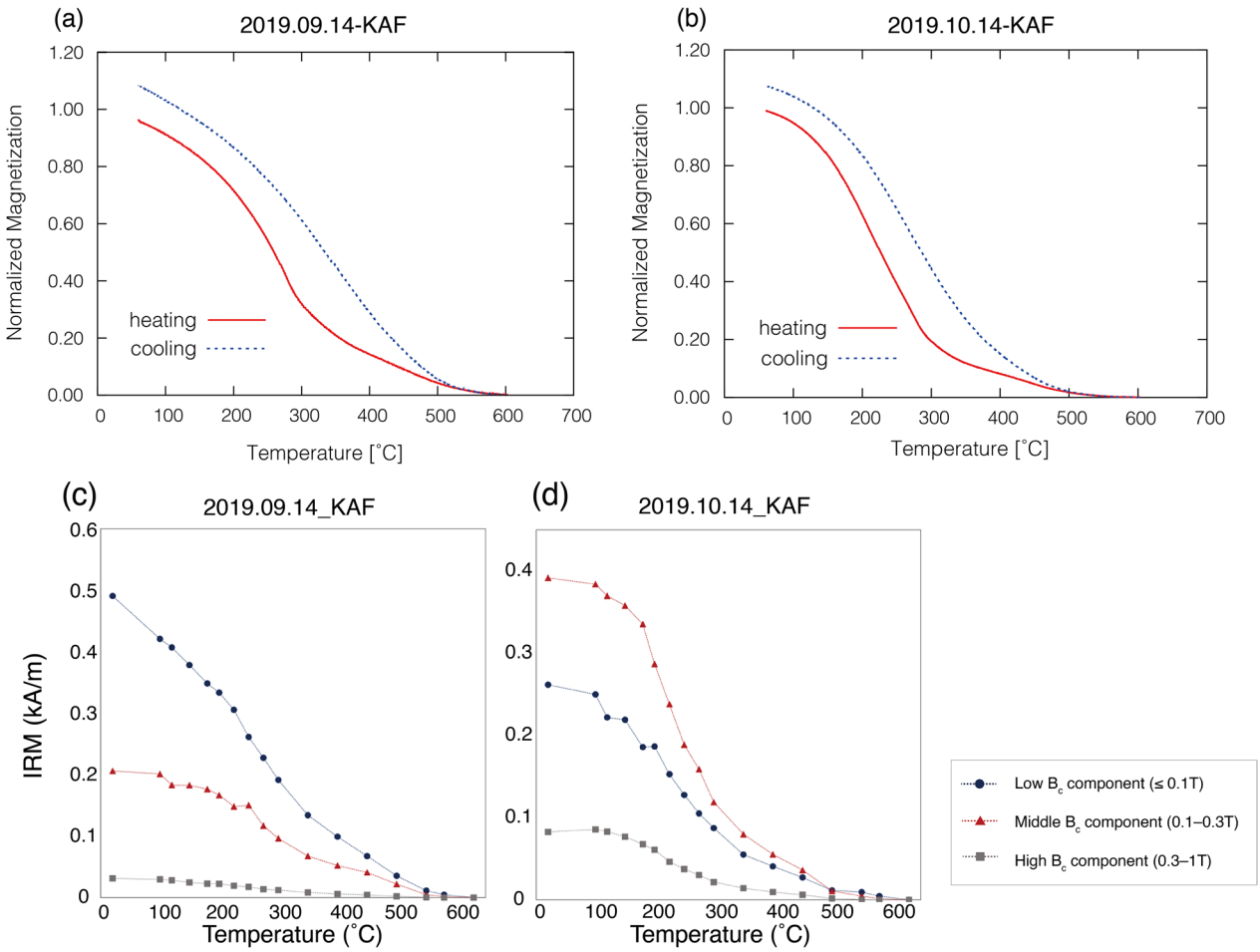

Fig. 1 Results of thermomagnetic analyses and thermal demagnetizations of a 3-axis composite IRM. **a** Thermomagnetic analysis in air for the sample of September 14, 2019. The red solid line is the heating curve and the blue dashed line is the cooling curve. **b** Result of thermomagnetic analyses in air for the sample of October 14, 2019. Legend is the same as **a**. **c** Result of thermal demagnetization of a 3-axis composite IRM for the sample of September 14, 2019. Coercivity components of ≤ 0.1 T, 0.1–0.3 T, and 0.3–1 T are shown by circles, triangles, and squares, respectively. **d** Result of thermal demagnetization of a 3-axis composite IRM for the sample of October 14, 2019

Thermomagnetic analyses and thermal demagnetizations of 3-axis IRM suggest that the major magnetic mineral in the volcanic ash samples used in this study is low T_c phase of 200–350 °C (Fig. 1a, b), which show a large change in coercivity (Fig. 1c, d).

The hysteresis measurements were performed for all of the volcanic ash samples. Hysteresis parameters (M_{rs}/M_s, B_c, and B_{cr}/B_c) were determined from the hysteresis loop measurements (Fig. 2a, b). The M_{rs}/M_s and B_c ranges were approximately 0.2–0.5 and 5–85 mT, respectively. These values indicate a clear positive correlation (Fig. 2c). On the diagram of M_{rs}/M_s vs. B_c (Fig. 2c), magnetic minerals governed by different magnetic anisotropies have their own trends (e.g., Wang and Van der Voo 2004). For this reason, the domain state was not determined by this diagram alone, but should be discussed based on the M_{rs}/M_s vs. B_{cr}/B_c diagram (Day plot: Day et al. 1977) as shown in Fig. 2d. The values of B_{cr}/B_c were 1.2–4.3. In general, high M_{rs}/M_s values and low B_{cr}/B_c values originate from a high SD fraction (low multi-domain (MD) fraction), thereby indicating that the high M_{rs}/M_s values (and the high B_c values) mean the size distribution of magnetic grains shifts finer (Dunlop 2002a and b).

Figure 2a, b shows hysteresis loops for the samples of September 14 and October 14, 2019 (Note that the two samples are the same as those in Fig. 1). The sample of October 14, 2019 indicates a clear increase in M_{rs}/M_s and B_c (Fig. 2b) compared to the sample of September 14, 2019 (Fig. 2a). The observed increase in M_{rs}/M_s and B_c appears to be consistent with the clear coercivity increase of the low unblocking-temperature component observed in the thermal demagnetizations of 3-axis IRM (Fig. 1c, d).

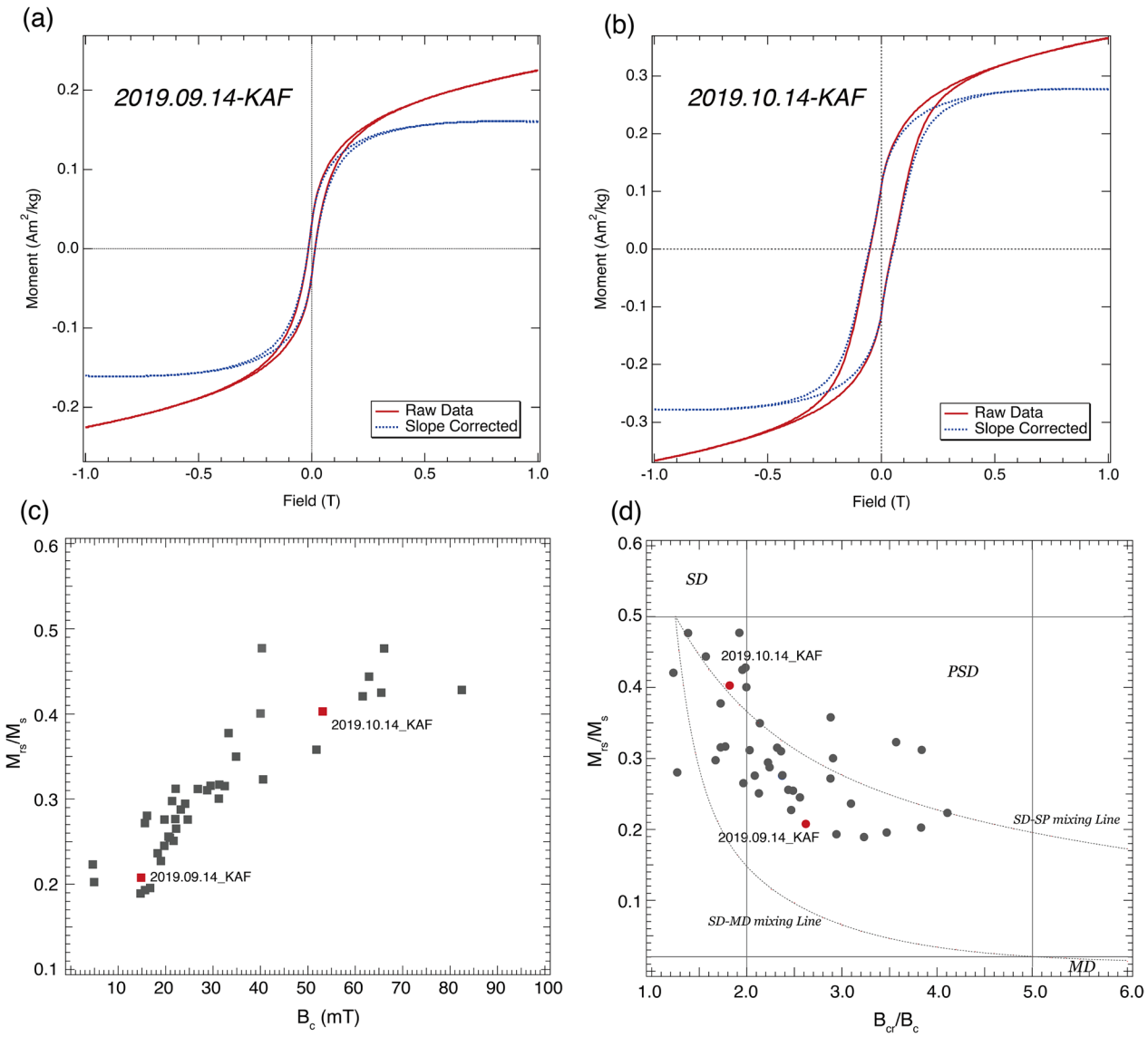

Fig. 2 Results of hysteresis measurement. **a**, **b** Examples of hysteresis loops. The red solid line is the measured hysteresis loop (raw data). The blue dashed line is the corrected loop for the effect of paramagnetic minerals. **c** Ratio of the saturation remanent magnetization to saturation magnetization (M_{rs}/M_s) vs. coercivity (B_c). **d** M_{rs}/M_s vs. coercivity of remanence to coercivity (B_{cr}/B_c). The upper left in the plot is single-domain (SD) region, while the lower right is closer to the multi-domain (MD) grain size. The two dotted lines are the SD–superparamagnetic (SP) mixing line (top) and the MD–SD mixing line (bottom) (Dunlop 2002a, b)

FORC measurements were performed on all volcanic ash samples. Representative results are shown in Fig. 3 and the other results are in Additional file 1: Fig. S6. Similar to the results of the hysteresis measurements, variations of B_C and B_U were observed in each sample. Overall, B_U tended to spread up and down at lower values of B_C. In addition, some samples contained magnetic grains with B_C values greater than 0.1 T, which had narrower B_U ranges. The parameters (B_C and B_U) obtained from the FORC diagram indicate the coercive force and interaction, respectively. According to Roberts et al. (2018), a low B_C value with a large spread of B_U can be interpreted as MD grains, while a high B_C value with a narrow distribution of B_U can be interpreted as SD grains. The FORC results of the samples in this study indicate that MD grains were present throughout the eruption period, with additional periods of predominant SD grains.

Figure 3 shows an FORC diagram for the volcanic ash samples collected from September to October 2019.

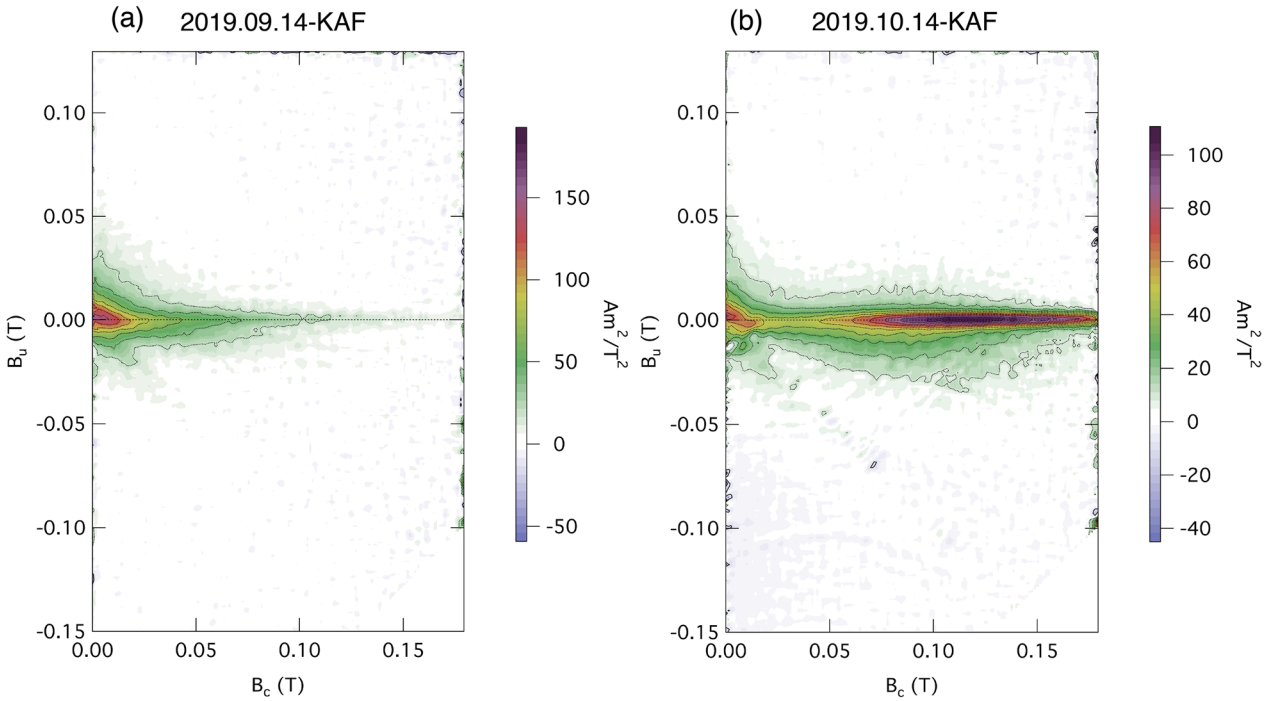

Fig. 3 Results of FORC measurement. **a** FORC diagram for the sample of September 14, 2019, collected from the KAF station. **b** FORC diagram for the sample of October 14, 2019, collected from the KAF station. Ash samples from October 14 indicate the presence of non-interacting SD grains with high coercivity and a narrow range of B_u values

The FORC diagram for the sample of October 14, 2019 (Fig. 3b) indicate the non-interacting SD grains with high coercivities compared to the sample of September 14, 2019 (Fig. 3a). As noted above, the sample of October 14, 2019 indicates a clear increase in M_{rs}/M_s and B_c (Fig. 2b) compared to the sample of September 14, 2019 (Fig. 2a). The increase in M_{rs}/M_s and B_c can be explained by the non-interacting SD grains.

Especially in late January and early to mid-February 2020, the dominance of SD grains with high coercivities are observed. The results for September 14, 2019 (Fig. 3a) and April 29, 2020 (Additional file 1: Fig. S6) had ranges of B_U values at low B_C values (< 0.05 T) that can be interpreted as the dominance of pseudo-single domain (PSD) and/or MD grains. For most of the samples, PSD and/or MD-like characters were identified.

SEM observations with EDS analysis revealed Ti-rich and Ti-poor titanomagnetite grains exist in the two samples (Additional file 1: Fig. S7). Ti-rich titanomagnetite grains are small in size (approximately < 1 μm), and they are recognized in the bubble-fractured volcanic glass. On the other hand, the 10–20 μm grain contains ilmenite–magnetite (Ti-poor titanomagnetite) lamellae (Additional file 1: Fig. S7).

The measured hysteresis parameters of M_{rs}/M_s and B_c were not constant throughout the eruption period. Figure 4 shows the temporal variation in M_{rs}/M_s for the 1-year eruption period. M_{rs}/M_s occasionally exhibited a large increase, which is followed by a decrease to typical values (approximately $M_{rs}/M_s < 0.32$, Fig. 4). It is also noted that high M_{rs}/M_s values appear to be correlated with the periods of volcanic glow. This matter is discussed in the next section.

Discussion

Temporal changes in rock magnetic properties

The thermomagnetic analyses and thermal demagnetizations of 3-axis IRM indicate that the volcanic ash samples contain two magnetic minerals, a low T_c phase of 200–350 °C and a high T_c phase of ~ 500 °C (Fig. 1). Both of the thermomagnetic analyses and thermal demagnetizations of 3-axis IRM indicate that dominant magnetic mineral is the low T_c phase (Fig. 1). As shown in Additional file 1: Fig. S7, Ti-rich and Ti-poor titanomagnetite grains were identified in the SEM observations with EDS analysis. Therefore, we concluded that the low and high T_c phases correspond to Ti-rich titanomagnetite and Ti-poor titanomagnetite, respectively. It should be also notified that the low T_c phase, which is considered to be Ti-rich titanomagnetite, is dominant for most of the samples ejected during the 1-year eruption.

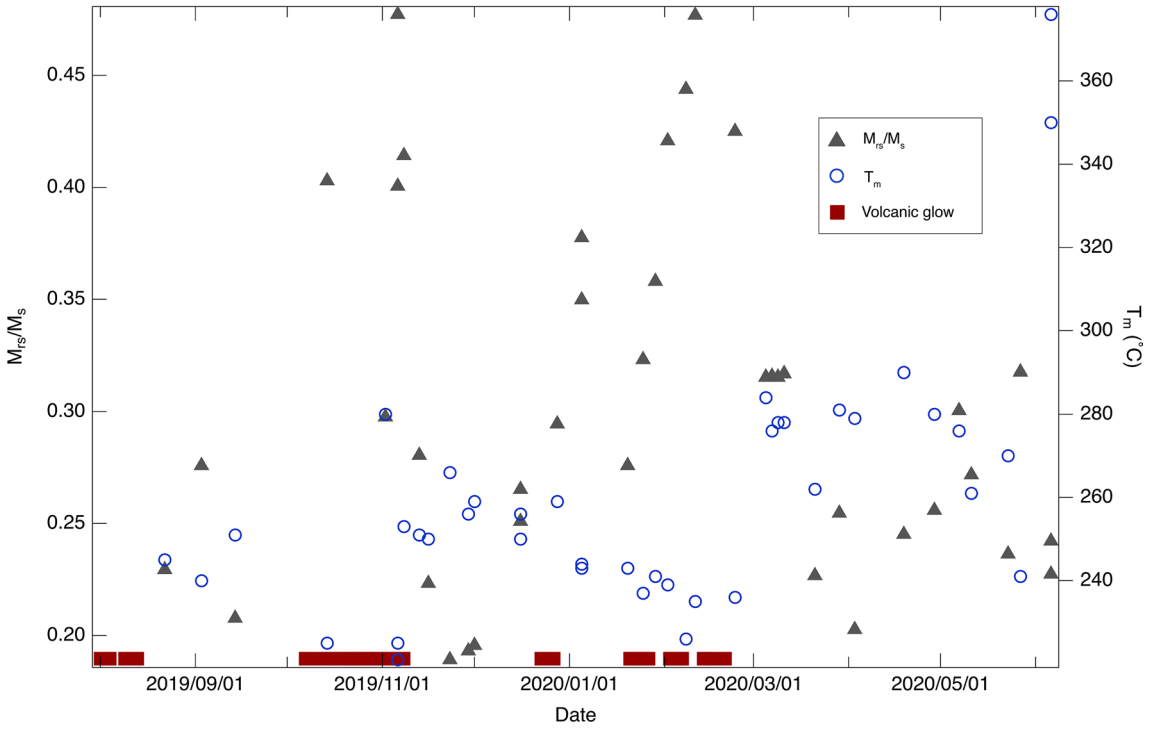

Fig. 4 Hysteresis parameters (M_{rs}/M_s) and the median destructive temperature from the thermomagnetic curve. T_m is the temperature given by $M_s(T_m) = 0.5\ M_{s0}$, where $M_s(T)$ is the saturation magnetization M_s at temperature T and M_{s0} is the M_s value at room temperature. Gray triangles denote M_{rs}/M_s and blue circles indicate T_m. Red squares indicate the day when the volcanic glow was observed. High M_{rs}/M_s values indicate the predominance of SD grains. Low T_m values indicate higher titanium contents

Temporal variation of M_{rs}/M_s (Fig. 4) and hysteresis parameters on the two diagrams (Fig. 2c, d) reveal that the domain state is changing with time. It is clear that M_{rs}/M_s and B_c have a linear correlation (Fig. 1c), and both parameters increase or decrease depending on the timing of the eruption. As mentioned above, the low T_c phase is dominant for the ash samples throughout the 1-year eruption period. Therefore, the changes in M_{rs}/M_s and B_c mainly reflect the change of domain state of the low T_c phase, which is regarded as Ti-rich titanomagnetite.

The two hysteresis loops shown in Fig. 2a, b are evidently constricted (wasp-waisted), indicating coexisting components with different coercivities. As noted above, the ash sample contains two T_c phases (low T_c and high T_c phases). In addition, the thermal demagnetizations of 3-axis IRM also indicate that two unblocking-temperature components were recognized, which correspond to the two T_c phases. Therefore, the constriction of the hysteresis loops appears to result from the mixing of two T_c phases. However, as noted above, the low T_c phase is dominated for most of the samples. Therefore, large change in hysteresis measurements is mainly related to the low T_c phase.

The FORC diagram for the sample of October 14, 2019 (Fig. 3b) shows the non-interacting SD grain, in addition to the MD character. The non-interacting SD character can be also identified in the sample of January 22, 2020 at SAK site and February 2 and 11, 2020 at KAF site (see Additional file 1: Fig. S6). The contribution of non-interacting SD grains is observed for the samples showing high M_{rs}/M_s and high B_c. Therefore, we consider that the high M_{rs}/M_s and high B_c originated from the non-interacting SD grains. In the thermal demagnetizations of 3-axis IRM, the low unblocking-temperature component show a higher coercivity for the high M_{rs}/M_s and high B_c periods (Fig. 1d). Therefore, we consider the non-interacting SD grains are Ti-rich titanomagnetite.

The increased SD fraction may be caused by a possible supply of non-interacting SD titanomagnetite. However, this possibility is not plausible, because the M_s values per unit mass do not show a correlation with the variation in M_{rs}/M_s (Additional file 1: Fig. S8).

As discussed later, a small Ti content change is observed for the low Tc phase (Additional file 1: Fig. S4). A change in Ti content may change coercivity of titanomagnetite grains. However, such small change in Ti content cannot give an explanation for the large variation in M_{rs}/M_s and B_c (Figs. 2c, d, and 4).

Overall, during the period of high M_{rs}/M_s shown in Fig. 4, the hysteresis loops demonstrate an SD-like

character (Fig. 2b), which is well-explained by the non-interacting SD grains (Fig. 3b). For the high M_{rs}/M_s periods, the coercivity increase is also recognized for the low unblocking-temperature component of the samples (Fig. 1d). SEM observations with EDS analysis show that small grains of < 1 μm are Ti-rich titanomagnetite. Therefore, these data indicate the non-interacting SD grains are Ti-rich titanomagnetite. We conclude that the high M_{rs}/M_s values result from the non-interacting SD Ti-rich titanomagnetite.

Potential link between rock magnetic properties and volcanic stages

Magmatic activity in the first crater of Aso Nakadake volcano began on July 26, 2019, and eruptions continued until June 15, 2020, with multiple pauses. During the active period, a large amount of ashfall, increases in volcanic gases, and increases in volcanic glow events over the crater were observed (Miyabuchi et al. 2021). Since volcanic glow produces bright illumination above a crater when hot magma or volcanic gas is present, it is reasonable to assume that volcanic glow is observed when volcanic activity is enhanced. Volcanic glow events were observed frequently from late July to early August 2019, from early October to mid-November, late December 2019, and from late January to late February 2020. As shown in Fig. 4, the high M_{rs}/M_s period coincide with the observed volcanic glow periods.

The results of thermomagnetic analysis and the Curie temperature estimates indicate that the Curie temperature of Ti-rich titanomagnetite varies slightly (Additional file 1: Fig. S4, Table S1). For a more quantitative investigation on the thermomagnetic curves, the median destructive temperature (T_m) of induced strong-field magnetization at room temperature was adopted as a proxy (Fig. 4). The T_m values were inversely correlated with M_{rs}/M_s (Fig. 5) and several tens of °C lower during the period of volcanic glow observed than during the rest of the study period, indicating that Ti-rich titanomagnetite with slightly higher Ti content crystallized during the period of volcanic glow observed. Thus, the crater interior during the high M_{rs}/M_s (volcanic glow observed) period changed to physical conditions that allowed SD Ti-rich titanomagnetite to crystallize.

Here we discuss the physical conditions inside a conduit. If we assume the pressure is constant throughout the eruption period, a higher temperature yields a higher Ti content of titanomagnetite based on Buddington and Lindsley (1964). Equivalently, if we assume the temperature is constant, a lower pressure gives a higher Ti content of titanomagnetite. Thus, the temperature of the magma head may be higher with the constant depth of the magma head, or the depth of the magma head may be shallower with the constant temperature. Such changes in physical conditions could have caused the volcanic glow events as well as the changes in rock-magnetic properties of the ash samples.

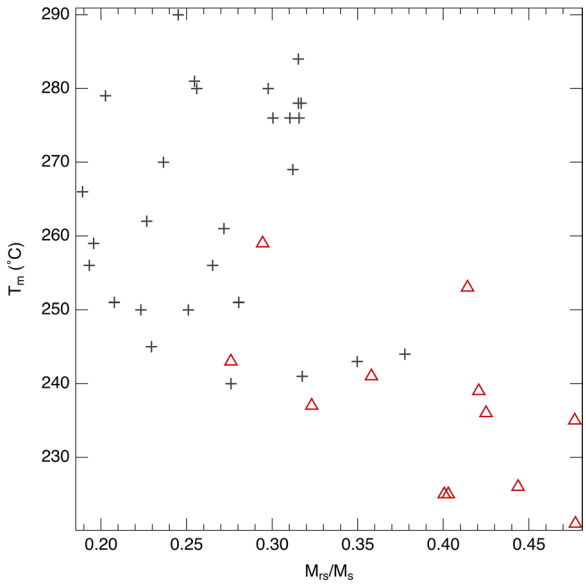

Fig. 5 T_m vs. M_{rs}/M_s of the ash samples. The HOND and KAF samples from June 6, 2020, in which no Ti-rich titanomagnetite was identified, were removed. Red triangles denote volcanic ash results when volcanic glow event was observed and gray crosses indicate those collected otherwise

Mujin and Nakamura (2014) noted that, when the magma head was located deep inside the crater, relatively large grains crystallized due to depressurization and a low temperature gradient. They mentioned, when the magma head rose, fine grains formed under the effects of degassing, rapid cooling, and oxidation. The high M_{rs}/M_s period, characterized by SD Ti-rich titanomagnetite with a slightly higher Ti content (Fig. 5), might be consistent with the magma head shallowing in the latter explanation. It is essential to compare the findings of this study with physical observations in the future studies. This study indicates that the temporal change in the rock-magnetic properties of volcanic ash can be used to investigate eruption processes. The 2019–2020 eruption of Aso Nakadake volcano was only ash eruption and we did not observe the precursor phenomena to a Strombolian eruption. In the future, we will perform a detailed study of the 2014–2015 eruption of Aso Nakadake volcano, which was accompanied by a Strombolian eruption.

Conclusions

In this study, rock-magnetic analyses were performed on volcanic ashes ejected by intermittent eruptions of the Aso Nakadake volcano from July 2019 to June 2020.

Ti-rich and Ti-poor titanomagnetite grains are included in the volcanic ash samples, where Ti-rich titanomagnetite is dominant. The hysteresis properties varied depending on the timing of the eruption. The higher M_{rs}/M_s and B_c values, combined with FORC diagrams, are indicative of the non-interacting SD grains. Thermomagnetic analyses and thermal demagnetizations of 3-axis IRM suggest that the non-interacting SD grains are Ti-rich titanomagnetite. The results of this study indicate that the high M_{rs}/M_s (high B_c) values coincide with the observed volcanic glow events. The temporal change in hysteresis properties of volcanic ash would reflect the physical conditions within the crater during the eruption.

Abbreviations

AYFC	National Aso Youth Friendship Center
FORC	First-order reversal curve
HOND	Hondo observatory
IRM	Isothermal remanent magnetization
JMA	Japan Meteorological Association
KAF	Kako-fuchi
KCC	Center for Advanced Marine Core Research, Kochi University
MD	Multi-domain
SAK	Sakanashi
SD	Single domain
VSM	Vibrating sample magnetometer

Supplementary Information

The online version contains supplementary material available at https://doi.org/10.1186/s40623-023-01783-x.

Additional file 1: Figure S1. Processes of Aso Nakadake Volcano activity, modified from Kawakatsu et al. (2000). **Figure S2.** Locality map of the Aso Nakadake Volcano and sampling points. The distances and directions of Kako-fuchi (KAF), the Hondo Observatory (HOND), Sakanashi (SAK), and the National Aso Youth Friendship Center (AYFC) from the first crater of the Aso Nakadake Volcano are approximately 250 m WSW, 1000 m SW, 7000 m NE, and 4400 m NNE, respectively. KAF and HOND are the observation stations of the Aso Volcanological Laboratory, Kyoto University. **Figure S3.** Comparison of air and vacuum atmosphere measurements in thermomagnetic analysis. No significant variation was observed in both vacuum and air atmosphere measurements. **Figure S4.** Results of strong-field thermomagnetic analyses (heating curve) of all samples. For a few exceptions, most of the thermomagnetic curves are characterized by two T_c phases. **Figure S5.** The result of thermal demagnetization of a 3-axis composite IRM. Coercivity components $\leq$ 0.1 T, 0.1–0.3 T, and 0.3–1 T are shown by circles, triangles, and squares, respectively. **Figure S6.** First-order reversal curve diagrams of the measured ash samples. The samples shown in Fig. 2 are omitted in this figure. The diagrams are arranged in chronological order. The results for the ash samples collected at (a) the Kako-fuchi (KAF) site, (b) the Sakanashi (SAK) site, and (c) the Hondo Observatory (HOND) site. **Figure S7.** The results of Scanning Electron Microscope (SEM) observation of 20191014_KAF ash. These photos are back-scattered images (BEIs). Left image: the white grain is titanium-poor titanomagnetite, which probably crystallized deep within the fire channel and formed ilmenite lamellae. Right image: white particles are titanium-rich titanomagnetite crystallized in volcanic glass (dark shard with curved, bubble-fractured edges). **Figure S8.** M_s vs. M_{rs}/M_s for the ash samples. No clear correlation has been recognized between M_{rs}/M_s and M_s. **Table S1.** Summary of rock-magnetic properties of the ash samples.

Acknowledgements
We would like to thank Hidetoshi Shibuya, Akihiko Yokoo, Mitsuru Ustugi and Satoko Ishimaru for their helpful discussions on this research. We also thank Yuhji Yamamoto and Tadahiro Hatakeyama for their assistance in conducting the measurements at KCC. We would like to thank Masaki Takaya and Hiroshi Isobe for their great help in preparing and observing the thin sections. We are grateful to Geoffrey Lerner and two anonymous reviewers for their constructive comments on the manuscript. This study was performed under the cooperative research program of the Center for Advanced Marine Core Research, Kochi University (No.19B064, 20A013 and 20B011). This study was also supported by the Earthquake Research Institute, University of Tokyo (No. ERI JURP 2021-KOBO23).

Author contributions
CA treated the samples, conducted all experiments, and wrote the manuscript. TO collected all ash samples and assisted in constructing the framework of this study and the manuscript. SY assisted in correcting and treating the samples and rock-magnetic experiments. NM assisted with the rock-magnetic experiments and drafted the manuscript. All authors read and approved the final manuscript.

Funding
This study was supported by the Earthquake Research Institute, University of Tokyo (No. ERI JURP 2021-KOBO23).

Declarations

Ethics approval and consent to participate
Not applicable.

Consent for publication
Not applicable.

Competing interests
Not applicable.

Author details
[1]Aso Volcanological Laboratory, Kyoto University, Minami-Aso, Kumamoto 869-1404, Japan. [2]Present Address: Center for Advanced Marine Core Research, Kochi University, Nankoku, Kochi 783-8502, Japan. [3]Department of Earth and Environmental Science, Faculty of Advanced Science and Technology, Kumamoto University, Kumamoto 860-8555, Japan.

Received: 12 July 2022 Accepted: 11 February 2023
Published online: 20 February 2023

References

Anai C, Miyabuchi Y, Utsugi M, Yoshikawa S, Mozhizuki N, Shibuya H, Ohkura T (2021) Reappraisal eruptive age and classification of holocene volcanic products around Nakadake Crater, Aso volcano using paleomagnetic and rock magnetic methods. Bull Volcanol Soc Jpn. 66(3):171–186. https://doi.org/10.18940/kazan.66.3.171. (**in Japanese with English abstract**)

Bowles JA, Jackson MJ, Berquó TS, Sølheid PA, Gee JS (2013) Inferred time- and temperature-dependent cation ordering in natural titanomagnetites. Nat Comm. https://doi.org/10.1038/ncomms2938

Buddington AF, Lindsley DH (1964) Iron–titanium oxide minerals and synthetic equivalents. J Petrol 5(2):310–357. https://doi.org/10.1093/petrology/5.2.310

Day R, Fuller M, Schmidt VA (1977) Hysteresis properties of titanomagnetites: grain size and composition dependence. Phys Earth Planet Inter 13:260–267

Dunlop DJ (2002a) Theory and application of the Day plot (Mrs/Ms versus Hcr/Hc) 1. Theorical curves and tests using titanomagnetite data. J Geophys Res. https://doi.org/10.1029/2001JB000486

Dunlop DJ (2002b) Theory and application of the day plot (Mrs/Ms versus Hcr/Hc) 2. Application to data for rocks, sediments, and soils. J Geophys Res. https://doi.org/10.1029/2001JB000487
Dunlop DJ, Özdemir Ö (1997) Rock magnetism: fundamentals and frontiers (Cambridge studies in magnetism no. 3). Cambridge University Press, Cambridge. https://doi.org/10.1017/CBO9780511612794
Grommé CS, Wright TL, Peak DL (1969) Magnetic properties and oxidation of iron–titanium oxide mineral in Alae and Makaopuhi Lava Lakes, Hawaii. J Geophys Res 74:5277–5293
Hunt CP, Moskowitz BM, Banerjee SK (1995) Magnetic properties of rocks and minerals. In: Ahrens TJ (ed) Rock physics and phase relations a handbook of physical constants. Wiley, New York. https://doi.org/10.1029/RF003
Jackson M, Bowles JA (2014) Curie temperatures of titanomagnetite in ignimbrites: effects of emplacement temperatures, cooling rates, exsolution, and cation ordering. Geochem Geophys Geosys 15(11):4343–4368. https://doi.org/10.1002/2014GC005527
Japan Meteorological Agency (2020) annual volcanic activity report. https://www.data.jma.go.jp/svd/vois/data/tokyo/STOCK/monthly_v-act_doc/fukuoka/2020y/503_20y.pdf, Accessed Dec 2020
Kawakatsu H, Kaneshima S, Matsubayashi H, Ohminato T, Sudo Y, Tsutsui T, Uhira K, Yamasato H, Ito H, Legrand D (2000) Aso 94: Aso seismic observation with broadband instruments. Journal of Volcanologyand Geothermal Research, 101:129–154.
Knnot TR, Branney MJ, Reichow MK, Finn DR, Tapster S, Coe RS (2020) Discovery of two new super-eruptions from the yellowstone hotspot track (USA): is the yellowstone hotspot waning? Geology 48:934–938. https://doi.org/10.1130/G47384.1
Lowrie W (1990) Identification of Ferromagnetic minerals in a rock by coercivity and unblocking temperature properties. Geophys Res Lett 17(2):159–162. https://doi.org/10.1029/GL017i002p00159
Miyabuchi Y, Hara C (2019) Temporal variation in discharge rate and component characteristics of tephra-fall deposits during the 2014–2015 eruption of Nakadake first crater Aso, Volcano, Japan. Earth Planets Space 7(1):1. https://doi.org/10.1186/s40623-019-1018-6
Miyabuchi Y, Iizuka Y, Futa E, Ohkura T (2021) Precursor activity of the 2019–2020 Magmatic Eruption at Nakadake first crater, Aso volcano: insights from Ash fall deposits from early activity on May 3–5, 2019. Bull Volcanol Soc Jpn 66(3):157–169. https://doi.org/10.18940/kazan.66.3_157. (**in Japanese with English abstract**)
Mujin M, Nakamura M (2014) A nanolite record of eruption style transition. Geology 42(7):611–614. https://doi.org/10.1130/G3553.1
Risica G, Alessio DR, Fabio S, Paola DC, Massimo P, Stavros M, Mauro R (2020) Refining the Holocene eruptive activity at Tenirife (Canary Islands): the contribution of paleomagnetism. J Volcanol Geotherm Res. https://doi.org/10.1016/j.jvolgeores.2020.106930
Roberts AP, Zhao X, Harrison RJ, Heslop D, Muxworthy AR, Rowan CJ, Larrasoaña JC, Florindo F (2018) Signatures of reductive magnetic mineral diagenesis from unmixing of first-order reversal curves. J Geophys Res Solid Earth 123(6):4500–4522. https://doi.org/10.1029/2018JB015706
Wang D, Van der Voo R (2004) The hysteresis properties of multidomain magnetite and titanomagnetite/titanomagnemite in mid-ocean ridge basalts. Earth Planet Sci Lett 220:175–184. https://doi.org/10.1016/S0012-821X(04)00052-4

Publisher's Note